Available online at www.sciencedirect.com
SciVerse ScienceDirect
journal homepage: www.elsevier.com/locate/ijrefrig

Modeling and simulation of the transcritical CO_2 heat pump system

Kai-Hsiang Lin [a,b], Cheng-Shu Kuo [c], Wen-Der Hsieh [c], Chi-Chuan Wang [a,*]

[a] Department of Mechanical Engineering, National Chiao Tung University, Hsinchu 300, Taiwan
[b] Institute of Nuclear Energy Research, Taoyuan 325, Taiwan
[c] Green Energy Research Laboratories, Industrial Technology Research Institute, Hsinchu 310, Taiwan

ARTICLE INFO

Article history:
Received 3 February 2013
Received in revised form
1 August 2013
Accepted 5 August 2013
Available online 13 August 2013

Keywords:
Carbon dioxide
Gas cooler
System modeling
COP
Transcritical

ABSTRACT

In this study, a CO_2 transcritical cycle model without imposing any excessive constraints such as fixed discharge pressure and suction pressure is developed. The detailed geometrical variation of the gas cooler and the evaporator have been taken into account. The model is validated with the experimental measurements. Parametric influences on the CO_2 system with regard to the effect of dry bulb temperature, relative humidity, inlet water temperature, compressor speed, and the capillary tube length are reported. The COP increases with the dry bulb temperature or the inlet relative humidity of the evaporator. Despite the refrigerant mass flowrate may be increased with the inlet water temperature, the COP declines considerably with it. Increasing the compressor speed leads to a higher heating capacity and to a much lower COP. Unlike those of the conventional sub-critical refrigerant, the COP of the transcritical CO_2 cycle does not reveal a maximum value against the capillary tube length.

Modélisation et simulation du système de pompe à chaleur au CO_2 transcritique

Mots clés : Dioxyde de carbone ; Refroidisseur de gaz ; Modélisation du système ; Coefficient de performance ; Transcritique

1. Introduction

The carbon dioxide refrigeration systems first appeared in 1850 and were used thereafter for a very long period of time. With the advent of the halocarbon refrigerants, natural refrigerants like carbon dioxide were slowly phased out. However, as is well known that the synthetic refrigerants, either CFC, HCFC, or HFC, cast significant impact on the environment, thereby raising serious concerns to ban the utilization of the CFC/HCFC/HFC. Hence revisit of the natural refrigerants had caught a lot attention since 1990, and CO_2 is a potential candidate for having advantages like environment friendliness, low price, non-flammability and non-toxicity. On the other hand, despite CO_2 has some drawbacks such as a rather low critical temperature and an extremely high operational pressure, Lorentzen and Pettersen (1993), Lorentzen

* Corresponding author. E474, 1001 University Road, Hsinchu 300, Taiwan. Tel.: +886 3 5712121x55105; fax: +886 3 5720634.
E-mail addresses: ccwang@mail.nctu.edu.tw, ccwang@hotmail.com (C.-C. Wang).
0140-7007/$ – see front matter © 2013 Elsevier Ltd and IIR. All rights reserved.
http://dx.doi.org/10.1016/j.ijrefrig.2013.08.008

Nomenclature

A	surface area (m^2)
A_{capi}	cross section area in the capillary tube (m^2)
A_f	fin area (m^2)
A_o	total surface area in the airside (m^2)
A_p	tube area (m^2)
A_{pi}	inside tube area (m^2)
A_{po}	outside tube area (tube outside surface area) (m^2)
A_{pm}	mean tube area, given by $A_{pm} = (A_{po} - A_{pi})/(\ln(A_{po}/A_{pi}))$ (m^2)
b'_p	slope of a straight line between the outside and inside tube wall temperature (J kg^{-1} K^{-1})
b'_r	slope of the air saturation curve at the mean coolant temperature (J kg^{-1} K^{-1})
$b'_{w,m}$	slope of the air saturation curve evaluated at the mean water film temperature on the fin) (J kg^{-1} K^{-1})
$b'_{w,p}$	slope of the air saturation curve evaluated at the mean water film (J kg^{-1} K^{-1})
Bo	boiling number
COP	coefficient of performance
Cp	specific heat (J kg^{-1} K^{-1})
d_{cap}	capillary tube diameter (m)
d_i	inner diameter of the inner tube of gas cooler (m)
d_H	hydraulic diameter of the annulus in the gas cooler (m)
d_o	outer diameter of the inner tube of gas cooler (m)
f	friction factor
F	correction factor
G	mass flux (kg m^{-2})
h	heat transfer coefficient (W m^{-2} K^{-1})
$h_{o,w}$	total heat transfer coefficient for wet external fin (W m^{-2} K^{-1})
I_0	modified Bessel function of 1st kind, order 0
I_1	modified Bessel function of 1st kind, order 1
i	enthalpy (J kg^{-1})
i_{ai}	inlet enthalpy of air (J kg^{-1})
i_{ao}	outlet enthalpy of air (J kg^{-1})
i_{ri}	saturated air enthalpy evaluated at the refrigerant inlet temperature (J kg^{-1})
i_{rm}	saturated air enthalpy evaluated at the average refrigerant temperature (J kg^{-1})
i_{ro}	saturated air enthalpy evaluated at the refrigerant outlet temperature (J kg^{-1})
$i_{s,w,m}$	saturated air enthalpy evaluated at the condensate water film temperature (J kg^{-1})
Δi_m	log mean enthalpy difference (J kg^{-1})
K_0	modified Bessel function of 2nd kind, order 0
K_1	modified Bessel function of 2nd kind, order 1
k	thermal conductivity (W m^{-1} K^{-1})
k_f	thermal conductivity of the fin (W m^{-1} K^{-1})
k_c	thermal conductivity of the CO_2 (W m^{-1} K^{-1})
k_p	thermal conductivity of the tube (W m^{-1} K^{-1})
k_w	thermal conductivity of the water (W m^{-1} K^{-1})
L	length of gas cooler (m)
LMTD	log mean temperature difference (K)
LMHD	log mean enthalpy difference (J kg^{-1})
$\dot{m}$	mass flowrate (kg s^{-1})
M_T	parameter defined in Eq. (19) (m^{-1})
N_{com}	compressor speed, rev
n	segment number
Nu	Nusselt number
p	pressure (Pa)
P_l	longitudinal tube pitch (m)
P_t	transverse tube pitch (m)
Pr	Prandtl number
Q	heat transfer rate (Watt)
r_c	radius of the tube collar (m)
r_{eq}	equilibrium radius for circular fin (m)
Re	Reynolds number
RH	relative humidity
T	temperature (°C)
$T_{p,i,m}$	mean temperature of the inner tube wall of the fin-and-tube evaporator (°C)
$T_{p,o,m}$	mean temperature of the outer tube wall of the fin-and-tube evaporator (°C)
$T_{r,m}$	mean temperature of refrigerant coolant (CO_2) (°C)
U	overall heat transfer coefficient (W m^{-2} K^{-1})
$T_{w,m}$	mean temperature of the condensate water film (°C)
$U_{o,w}$	overall heat transfer coefficient of the wet surface (kg m^{-2} s^{-1})
V_{com}	swept volume of the compressor (m^3)
v	specific volume (m^3 kg^{-1})
W	power consumption of the compressor (W)
x	vapor quality
X	Lockhart–Martinelli parameter
x_p	thickness of the tube (m)
y_w	thickness of the condensate water film (m)
z	axial direction of the capillary tube (m)

Greek letters

δ_f	thickness of the fin (m)
ε	surface roughness in the capillary tube (m)
μ	dynamic viscosity (Pa s)
ρ	density (kg m^{-3})
ϕ	two-phase friction multiplier
$\eta_{f,wet}$	wet fin efficiency
η_{isen}	isentropic efficiency
η_v	volumetric efficiency

Subscripts

1	saturated region
2	superheated region
a	air
b	bulk
c	carbon dioxide
c,i	ith segment of carbon dioxide
dis	discharge
db	inlet dry bulb temperature
eva	evaporator
f	evaluated at film temperature
g	gas
h	heating
i	ith segment of heat exchanger
i	inlet or inner

in	inlet	tp	two phase
l	liquid phase	v	vapor phase
o	outlet	w	water
s	saturation	wet	wet
sp	single phase	wb	inlet wet bulb temperature
suc	suction	wall	wall
t	total		

(1994, 1995) and Riffat et al. (1996) had shown that the problem of the low critical temperature of the carbon dioxide can be effectively overcome by operating the system in the transcritical region. This had led to the revival of the CO_2 as a refrigerant and it is implemented as the transcritical carbon dioxide cycle with the condenser being replaced by a gas cooler.

There had been a number experimental studies associated with the performance of the transcritical CO_2 system (e.g. Stene, 2005; Cabello et al., 2008; Aprea and Maiorino, 2009). These studies provided valuable design information from the aspect of practical applications. For further examinations of the transcritical behaviors of the CO_2 system, some comprehensive system simulations with thermodynamics base and detailed component modeling may be helpful in practice. However, due to the transcritical nature of the CO_2, the performance of the carbon dioxide system will not be exactly the same as the conventional one. Hence the simulation models developed for the conventional systems cannot be directly employed to this system. There were some available system modeling concerning the system performance of the CO_2 transcritical cycle as tabulated in Table 1, including those by Kim et al. (2005), Yang et al. (2010), Sarker et al. (2004, 2006, 2009, 2010), Yokoyama et al. (2007), Wang et al. (2009) and Yamaguchi et al. (2011).

The abovementioned developed system model provided many in-depth contents about the transcritical features of the CO_2 system. Nevertheless the foregoing models all had some excessive constraints in the simulation, such as constant suction superheat, suction pressure, discharge pressure, or a given compressor power. Yet some of the modeling is thermodynamics base and lacked some detailed influence of the heat exchangers (gas cooler or evaporator). Note that the actual system response normally floats when the operating conditions of the heat exchangers vary. As a result, the actual response of the CO_2 system may not be so realistic due to excessive constraints. Hence it is the main purpose of this study to propose a comprehensive system model to relax all these restrictions, and to include some detailed modeling of the heat exchangers, including gas cooler and the fin-and-tube heat exchanger, that can take into account the complex variations of the geometrical parameters and inlet conditions.

Table 1 – Comparisons of the available CO_2 system simulation model.

Study	Gas cooler	Evaporator	Expansion device model	Inner HX	Excessive controlled conditions
Kim et al. (2005)	Water Tube-in-tube	Water Tube-in-tube	$\Delta i = 0$	Yes	P_{dis}, T_{sup}
Yang et al. (2010)	Water Shell-tube	Water Shell-and-tube	$\dot{W}_{exp} = G_r(i_3 - i_{4,is}) \times \eta_{exp,is} \times \eta_{exp,m}$	No	P_{dis}
Sarker et al. (2006)	Water Tube-in-tube	Water Tube-in-tube	$\Delta i = 0$	Yes	Maximum COP
Yokoyama et al. (2007)	Water Tube	Water Tube	$\Delta i = 0$	No	$\dot{m}_{Co_2}$, P_{eva}, $T_{ci,gc}$
Yamaguchi et al. (2011)	Water Tube-in-tube	Air Fin-and-tube	$\Delta i = 0$	Yes	W_{com}
Wang et al. (2009)	Water Tube-in-tube	Water Tube-in-tube	$\Delta i = 0$	No	Maximum COP
Sarker et al. (2004)	No description	No description	$\Delta i = 0$	Yes	T_{eva}, $T_{co,gc}$, Maximum COP
Sarker et al. (2009)	Water Tube-in-tube	Water Tube-in-tube	$\Delta i = 0$	No	P_{dis}, Degree of superheat
Sarker et al. (2010)	Water Tube-in-tube	Water Tube-in-tube	$\Delta i = 0$	No	P_{dis}, P_{suc}
This study	Water Tube-in-tube	Air Fin-and-tube	$\Delta i = 0$	No	No

2. Numerical method

The carbon dioxide heat pump system is shown in Fig. 1 and it is consisted of a gas cooler, an evaporator, a compressor, and an expansion device. Water is supplied to the gas cooler to absorb heat from CO_2 and the air at the ambient temperature enters the fin-and-tube evaporator. The gas cooler is a double-pipe heat exchanger as shown in Fig. 2(a) with a counter-flow arrangement (Fig. 2(b)) and a fin-and-tube heat exchanger having plain fin configuration in Fig. 2(c) is used as the evaporator. The expansion device in this study is a capillary tube as shown in Fig. 2(d). Further details of the components modeling is summarized in the subsequent sections.

2.1. *Gas cooler*

The gas cooler is a double-pipe heat exchanger with the water flowing in the annulus and the CO_2 flowing counter-currently along the inner tube as shown in Fig. 2(a). Some basic assumptions for analyzing the gas cooler are summarized as follows:

1. The pressure drop of the water and the carbon dioxide in the heat exchangers and connecting pipes are negligible.
2. The heat transfer process for the water within the gas-cooler is single-phase only.
3. Heat loss to the ambient is negligible.

With the tremendous property variation of the CO_2 at the transcritical region, the gas cooler must be discretized into tiny segments and the energy conservation equations in every segment must be employed. A prior sensitivity analysis of the influence of the segments on the overall accuracy was performed, and a total of 65 segments were used in the simulation (Yu et al., 2012). A schematic showing the variation of the temperature of the CO_2 and the water is shown in Fig. 2(b), where the subscript c denotes the CO_2 and w represents the water. The heat balance between the water and the CO_2 in each segment *i* can be expressed by the following equations:

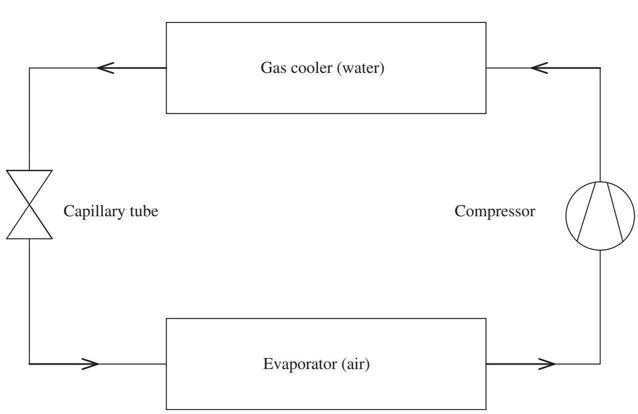

Fig. 1 – Schematic diagram of the CO_2 system. (a) Schematic of the gas cooler-tube in tube heat exchanger.(b) Counter flow arrangement of the gas cooler. (c) Schematic of the fin-and-tube evaporator. (d) Schematic of the capillary tube.

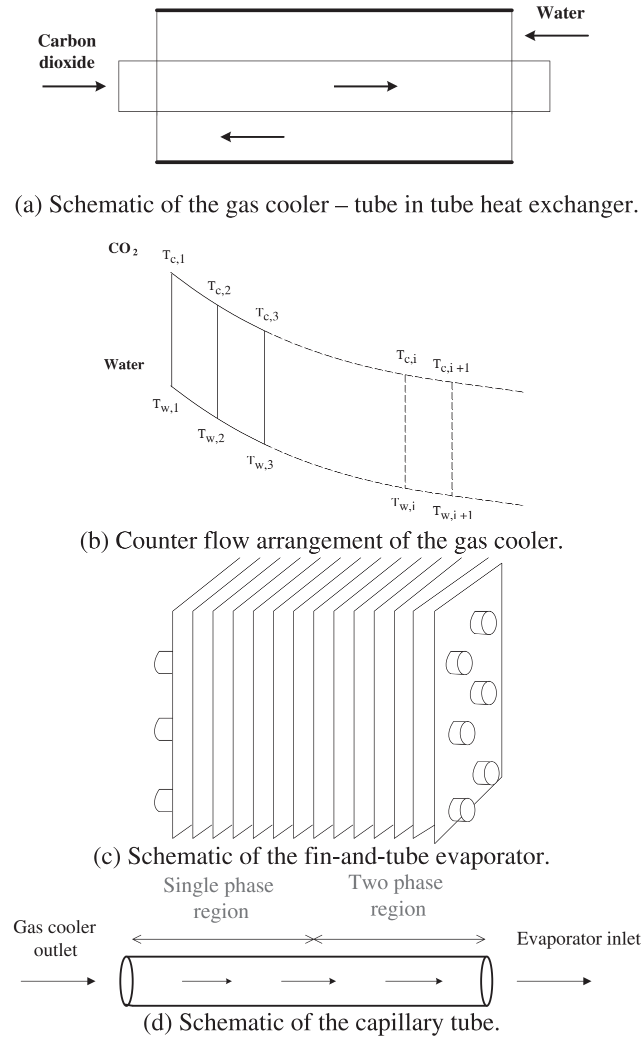

Fig. 2 – Schematics of the major components (a), (b): gas cooler; (c): evaporator; and (d) capillary tube.

$$Q_i = \dot{m}_c Cp_{c,i}(T_{c,i} - T_{c,i+1}) = \dot{m}_w Cp_{w,i}(T_{w,i} - T_{w,i+1}). \tag{1}$$

$$Q_i = (UA)_i \times (LMTD)_i. \tag{2}$$

The overall heat transfer coefficient is obtained from

$$\frac{1}{UA} = \frac{1}{h_w A_{o,i}} + \frac{\ln\frac{d_o}{d_i}}{2\pi k_{wall} L} + \frac{1}{h_c A_{i,i}}. \tag{3}$$

The physical properties of the CO_2 are a function of the local pressure and temperature, and the properties of the water are related to the local temperature. The relevant properties are obtained from REFPROP 8.0 (2007). The heat transfer coefficient of the CO_2 is based on the correlation of Dang and Hihara (2004), i.e.

$$h_c = Nu_c k_c / d_i. \tag{4}$$

$$Nu_c = \frac{\left(\frac{f_c}{8}\right)(Re_b - 1000)Pr_c}{1.07 + 12.7\sqrt{\frac{f_c}{8}}\left(Pr_c^{\frac{2}{3}} - 1\right)}. \tag{5}$$

where

$$\Pr = \begin{cases} \overline{Cp}_{b,c}\mu_{b,c}/k_{b,c}, & \text{for } Cp_{b,c} \geq \overline{Cp} \\ \overline{Cp}_{b,c}\mu_{b,c}/k_{f,c}, & \text{for } Cp_{b,c} < \overline{Cp} \text{ and } \mu_{b,c}/k_{b,c} \geq \mu_{f,c}/k_{f,c} \\ \overline{Cp}_{b,c}\mu_{f,c}/k_{f,c}, & \text{for } Cp_{b,c} < \overline{Cp} \text{ and } \mu_{b,c}/k_{b,c} < \mu_{f,c}/k_{f,c} \end{cases} \quad (6)$$

$$\overline{Cp} = \frac{i_{b,c} - i_{wall,c}}{T_{b,c} - T_{wall,c}}. \quad (7)$$

$$Re_b = \frac{Gd_i}{\mu_{b,c}}. \quad (8)$$

$$f_c = [1.82\log(Re_b) - 1.64]^{-2}. \quad (9)$$

where the subscript b represents the evaluation at the bulk temperature, wall is evaluated at the wall temperature and f denotes the value at the film temperature. The film temperature, T_f, is defined as $T_f = (T_b + T_{wall})/2$. In contrast, the heat transfer coefficient for the water side, h_w, is obtained via the Gnielinsk (1976) correlation:

$$h_w = Nu_w k_w/d_H. \quad (10)$$

$$Nu_w = \frac{\left(\frac{f_w}{8}\right)(Re_w - 1000)Pr_w}{1.07 + 12.7\sqrt{\frac{f_w}{8}}\left(Pr_w^{\frac{2}{3}} - 1\right)}. \quad (11)$$

where

$$f_w = [1.82\log(Re_w) \text{ -}1.64]^{-2}. \quad (12)$$

2.2. *Evaporator*

Heat transfer in the airside of the evaporator involves both heat and mass transfer. Thus, the enthalpy-based method proposed by Threlkeld (1970) is adopted. The heat transfer rate in the evaporator is calculated as

$$Q_{eva} = \dot{m}_a(i_{ai} - i_{ao}). \quad (13)$$

where i_{ai} and i_{ao} are the inlet and outlet enthalpy of the air flow. The rating equation of the dehumidifying heat exchanger, according to Threlkeld (1970), is:

$$Q_{eva} = U_{ow}A_o F \Delta i_m. \quad (14)$$

where U_{ow} is the enthalpy-based overall heat transfer coefficient, F is the correction factor and Δi_m is the log mean enthalpy difference. For counter flow arrangement, Δi_m is given as follows (Bump, 1963; Myers, 1967)

$$\Delta i_m = \frac{(i_{ai} - i_{ro}) - (i_{ao} - i_{ri})}{\ln\left(\frac{i_{ai} - i_{ro}}{i_{ao} - i_{ri}}\right)}. \quad (15)$$

The enthalpy-based overall heat transfer coefficient $U_{o,w}$ in Eq. (14) is evaluated as (Wang et al., 1997):

$$U_{o,w} = \left[\frac{b'_r A_o}{h_i A_{p,i}} + \frac{b'_p x_p A_o}{k_p A_{p,m}} + \frac{1}{h_{o,w}\left(\frac{A_{p,o}}{b'_{w,p}A_o} + \frac{A_f \eta_{f,wet}}{b'_{w,m}A_o}\right)}\right]^{-1}. \quad (16)$$

where

$$h_{o,w} = \frac{1}{\frac{Cp_a}{b'_{w,m}h_{c,o}} + \frac{y_w}{k_w}}. \quad (17)$$

Note that y_w in Eq. (17) is the thickness of the condensate water film. A constant of 0.005 inch of the condensate film was proposed by Myers (1967). In practice, y_w/k_w accounts only 0.5–5% comparing to $Cp_a/b'_{w,m}h_{c,o}$ and is often neglected by previous investigators (Wang et al., 1997). As a result, this term is not included in the final analysis. The wet fin efficiency in Eq. (16) is calculated as:

$$\eta_{wet,f} = \frac{2r_c}{M_T\left(r_{eq}^2 - r_c^2\right)} \times \left[\frac{K_1(M_T r)I_1(M_T r_{eq}) - K_1(M_T r_{eq})I_1(M_T r_c)}{K_1(M_T r_{eq})I_0(M_T r_c) + K_0(M_T r_c)I_1(M_T r_{eq})}\right]. \quad (18)$$

where

$$M_T = \sqrt{\frac{2h_{o,w}}{k_f\delta_f}} = \sqrt{\frac{2h_{c,o}}{k_f\delta_f}} \times \sqrt{\frac{b'_{w,m}}{Cp_a}}. \quad (19)$$

r_c is radius including collar and r_{eq} is the equivalent radius for circular fin. For the present plate fin geometry, Threlkeld (1970) recommended the following approximation:

$$r_{eq} = \sqrt{\frac{p_t \times p_l}{\pi}}. \quad (20)$$

Notice that the evaluation of wet fin efficiency is quite controversy in the open literature. Interested readers should refer to the article by Lin et al. (2001) for further discussion. The present study adopts the enthalpy-based wet fin efficiency. Also shown in Eq. (16), there are four quantities ($b'_{w,m}, b'_{w,p}, b'_p$, and b'_r) involving enthalpy-temperature ratios that must be evaluated. The quantities of b'_p, and b'_r can be calculated as:

$$b'_r = \frac{i_{s,p,i,m} - i_{r,m}}{T_{p,i,m} - T_{r,m}}. \quad (21)$$

$$b'_p = \frac{i_{s,p,o,m} - i_{s,p,i,m}}{T_{p,o,m} - T_{p,i,m}}. \quad (22)$$

The values of $b'_{w,p}$ and $b'_{w,m}$ are the slope of the saturated enthalpy curve evaluated at the outer mean water film temperature that is at the base surface and at the fin surface. Without loss of generality, $b'_{w,p}$ can be approximated by the slope of the saturated enthalpy curve evaluated at the base surface temperature (Wang et al., 1997). Unfortunately, there is no explicit way to determine $b'_{w,m}$, and it must be obtained by trial and error procedures. The evaluation procedure is as follows:

(1) Assume a value of $T_{w,m}$ and determine its corresponding value of $b'_{w,m}$.
(2) Obtain the overall heat transfer coefficient, $h_{o,w}$, from Eq. (17).
(3) Evaluate the wet fin efficiency from Eq. (18).
(4) Calculate the enthalpy-based overall heat transfer coefficient $U_{o,w}$ from Eq. (16).
(5) Calculate the $i_{s,w,m}$ using the following equation;

$$i_{s,w,m} = i - \frac{C_{p,a} h_{o,w} \eta_{wet,f}}{b'_{w,m} h_{c,o}} \left(1 - U_{o,w} A_o \left[\frac{b'_r}{h_i A_{p,i}} + \frac{x_p b'_p}{k_p A_{p,m}}\right]\right)(i - i_{r,m}). \tag{23}$$

(6) Determine $T_{w,m}$ at $i_{s,w,m}$. If it is not the same with the assumed value, assume a new value and repeat the procedure.

The detailed empirical correlations for various fin patterns of the sensible heat transfer coefficients $h_{c,o}$ in wet conditions were summarized by Wang (2000) and Wang et al. (2001). In this study, the plain fin geometry is used for the simulation and experimentation. Note that the corresponding plain fin correlation is from Wang et al. (1997) since the present simulation range and geometry falls within the scope of the test ranges of their data. The applicable range of their correlation is as follows:

P_t (transverse pitch): 25.4 mm,
P_l (longitudinal pitch): 22 mm.
Nominal tube diameter (tube diameter): 9.52 mm.
Frontal velocity: 0.3–4 m s^{-1}.
Relative humidity: 50–90%.

Calculation of the two-phase evaporation heat transfer coefficient is based on the Hihara and Tanaka correlation (2000) applicable for in-tube evaporation of the CO_2. i.e.

$$\frac{h_{eva,c}}{h_{lo}} = C_1 Bo + C_2 \left(\frac{1}{X_{tt}}\right)^{2/3}. \tag{24}$$

Where C_1 and C_2 are the empirical coefficients ($C_1 = 1.4 \times 10^4$, $C_2 = 0.93$) and X_{tt} is the Lockhart–Martinelli (1949) variable, and is given by

$$X_{tt} = \left(\frac{1-x}{x}\right)^{0.9} \left(\frac{\rho_{g,c}}{\rho_{l,c}}\right)^{0.5} \left(\frac{\mu_{l,c}}{\mu_{g,c}}\right)^{0.1}. \tag{25}$$

h_{lo} is the heat transfer coefficient corresponding to the liquid phase flowing at the total mass flowrate, calculated from the Dittus–Boelter equation:

$$h_{lo} = 0.023 Re_{l,c}^{0.8} Pr_{l,c}^{0.4} \frac{k_{l,c}}{d_i}. \tag{26}$$

where $k_{l,c}$ is the liquid thermal conductivity of the CO_2. Notice that the two-phase CO_2 in the evaporator may fully evaporate to become superheated vapor where only single phase heat transfer takes place. As a consequence, simulation of the evaporator must be divided into two regions, namely the two-phase region and the single phase region. The total heat transfer surface of the fin-and-tube heat exchanger A is equal to:

$$A = A_1 + A_2. \tag{27}$$

Where the subscript 1 represents the two-phase evaporation region and 2 denotes the superheated single-phase region. The superheated single-phase heat transfer coefficient can be obtained from the Gnielinsk (1976) correlation (Eq. (11)).

2.3. Capillary tube

The expansion process is via a capillary tube in which an isenthalpic process is fulfilled. A schematic of the capillary tube is shown in Fig. 2(d). The continuity and the energy equations are as follows:

$$\dot{m}_{c,o} - \dot{m}_{c,i} = 0. \tag{28}$$

$$\dot{m}_{c,o} i_{c,o} - \dot{m}_{r,i} i_{c,i} = 0. \tag{29}$$

As shown in Fig. 2(d), the capillary tube undergoes both single- and two-phase process. It is imperative to calculate the total pressure drop of the capillary tube. The pressure drop of single-phase region can be easily obtained. For the two-phase region, the homogenous two-phase flow model is adopted with the mean two-phase viscosity being evaluated as (McAdams et al., 1942):

$$\frac{1}{\mu_{tp}} = \frac{1-x}{\mu_l} + \frac{x}{\mu_g}. \tag{30}$$

where x is the vapor quality and the subscripts tp, l, and g represents the two-phase, the saturated liquid, and the saturated vapor, respectively.

The variation of the pressure gradient in the two-phase region comprises the wall friction and the flow acceleration, and is calculated as (Agrawal et al., 2011):

$$\frac{dp}{dz} = -G^2 \left(f_{tp} \frac{\upsilon}{2d_{cap}} + \frac{d\upsilon}{dz}\right). \tag{31}$$

where p is the local pressure in the capillary tube, G is the mass flux, υ is the specific volume, and d_{cap} is the diameter of the capillary tube. The two-phase friction factor is evaluated based on the Lin et al.'s correlation (1991):

$$f_{tp} = \phi_{tp} f_{sp} \left(\frac{\upsilon_{sp}}{\upsilon_{tp}}\right). \tag{32}$$

$$\phi_{tp} = \left[\frac{(8/Re_{tp})^{12} + \left(A_{tp}^{16} + B_{tp}^{16}\right)^{-3/2}}{(8/Re_{sp})^{12} + \left(A_{sp}^{16} + B_{sp}^{16}\right)^{-3/2}}\right]^{1/12} \left[1 + x\left(\frac{\upsilon_g}{\upsilon_l} - 1\right)\right]. \tag{33}$$

$$A = 2.457 \ln\left(\frac{1}{(7/Re_{tp})^{0.9} + 0.27\varepsilon/d_{cap}}\right), \quad B = \frac{37530}{Re_{tp}}. \tag{34}$$

$$Re_{tp} = \frac{G d_{cap}}{\mu_{tp}}. \tag{35}$$

where f is the Fanning friction factor, ϕ is the two-phase frictional multiplier and the subscript sp represents the single phase and Re is the Reynolds number.

2.4. Compressor

The continuity and the energy equations of the compressor are as follows:

$$\dot{m}_{c,o} - \dot{m}_{c,i} = 0. \tag{36}$$

$$\dot{m}_{c,o} i_{c,o} - \dot{m}_{c,i} i_{c,i} = W_{com}. \tag{37}$$

The isentropic efficiency η_{isen} and the volumetric efficiency η_v are defined as follows:

$$\eta_{isen} = \frac{i_{c,isen} - i_{c,i}}{i_{c,o} - i_{c,i}}. \quad (38)$$

$$\eta_v = \frac{\dot{m}_{c,i}}{\rho_{c,i} V_{com} N_{com}}. \quad (39)$$

where V_{com} is swept volume of the compressor, N_{com} is the compressor speed and $\rho_{c,i}$ is the inlet density into the compressor. The volumetric efficiency η_v and the isentropic efficiency η_{isen} are estimated from the correlations by Sarkar et al. (2010):

$$\eta_v = 0.9207 - 0.0756\left(\frac{p_{dis}}{p_{suc}}\right) + 0.0018\left(\frac{p_{dis}}{p_{suc}}\right)^2. \quad (40)$$

$$\eta_{isem} = -0.26 + 0.7952\left(\frac{p_{dis}}{p_{suc}}\right) - 0.2803\left(\frac{p_{dis}}{p_{suc}}\right)^2 + 0.0414\left(\frac{p_{dis}}{p_{suc}}\right)^3 - 0.0022\left(\frac{p_{dis}}{p_{suc}}\right)^4. \quad (41)$$

where p_{dis} is the compressor discharge pressure, and p_{suc} is the compressor suction pressure.

2.5. *Numerical procedure*

The system model is consisted of four major modules (compressor, capillary tube, gas cooler, and evaporator). Implementation of the system model requires the integration of the separate modules. The most influential design

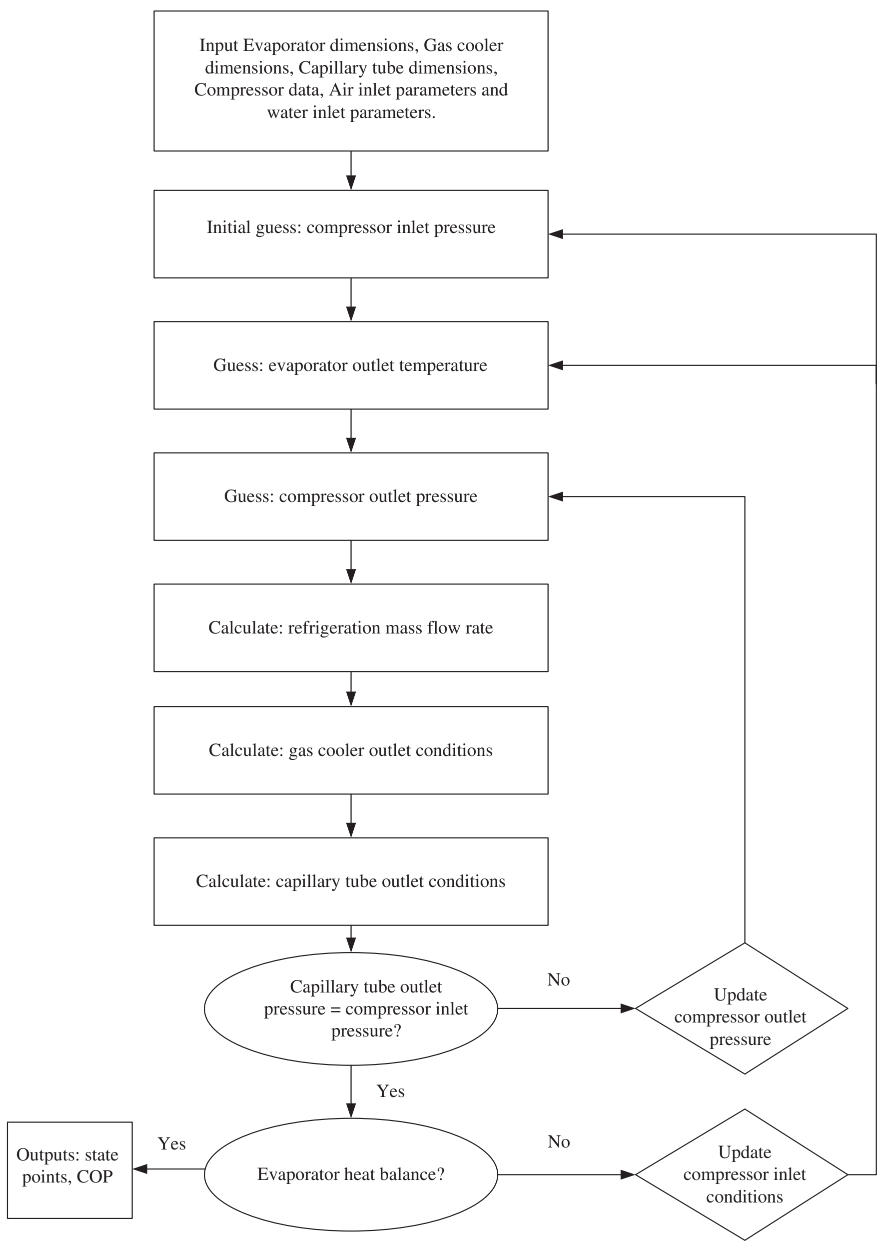

Fig. 3 – Flow chart for the simulation model. (a) Exterior (back view). (b) Exterior (front view). (c) Schematic of the system and sensor locations.

parameters are the refrigerant mass flowrate, the discharge pressure, the suction pressure, and the suction temperature before entering the compressor. However, these design parameters are inter-connected. Thus, it is necessary to obtain these design parameters by iteration. The iteration of the system modeling requires the balance of the high pressure side (compressor, gas cooler, and the capillary tube) and the low pressure side (evaporator). Calculation was first performed in the compressor to obtain the CO_2 mass flowrate in the high pressure side. The mass flowrate in the high pressure side is then used consecutively to obtain the exit condition of the gas cooler, the capillary tube, and the evaporator. The relevant exit conditions are then used to check whether the initial guesses were met. The solution algorithm can be seen from Fig. 3. Relevant procedures are summarized as follows:

a. (1) Input the geometrical parameters and the configurations of the major components (gas cooler, evaporator, capillary tube, and compressor speed).
   (2) Prescribe the inlet conditions (the dry, wet bulb temperature and the frontal velocity) of the incoming air into the evaporator.
   (3) Prescribe the inlet water condition into the gas cooler (inlet water temperature, and the mass flowrate)
   (3) Guess the inlet suction temperature, the suction pressure, and the discharge pressure.
b. Based on the compressor model, evaluate the mass flowrate $\dot{m}_{c,comp}$ across the compressor and the outlet state (enthalpy and the discharge temperature) of the compressor.
c. From the exit condition of the compressor as the inlet state of the CO_2 into the gas cooler, calculate the heat transfer rate, pressure drop, and the exit state of the gas cooler. Note that due to the tremendous variation of the CO_2 property, the gas cooler is further divided into tiny segments.
d. From the exit condition of the gas cooler and the mass flowrate, $\dot{m}_{c,capi} = \dot{m}_{c,comp}$, to estimate the exit pressure of the capillary tube. If the exit evaporating pressure is not equal to the originally guessed suction pressure, repeat process a.
e. Based on the exist sate of the capillary tube, calculate the heat transfer rate, friction loss, and the exit state of the evaporator. Check the exit temperature and the capacity of the gas cooler against the summation of the evaporator capacity and the compressor work. If these values are not the same, readjust the initial guesses of suction temperature and the gas cooler pressure. Repeat the process a to f until it converges.
g. End the system program and dump the calculated results.

3. Experimental setup and verification of experiments and simulation

An experimental CO_2 system is made available to verify the proposed model. The CO_2 system contains a semi-hermetic compressor (Danfoss TN 1410 reciprocating-type compressor), a gas-cooler, a capillary tube and a fin-and-tube evaporator. A layout of the instrumented test facility is shown in Fig. 4(a),(b) and (c) depicts the location of the measurements. A magnetic flowmeter is used to record the flowrates of water in the gas cooler. The magnetic flowmeter was calibrated in advance with a calibrated accuracy of 0.002 L s^{-1}. Two absolute pressure transducers are installed at the inlet of

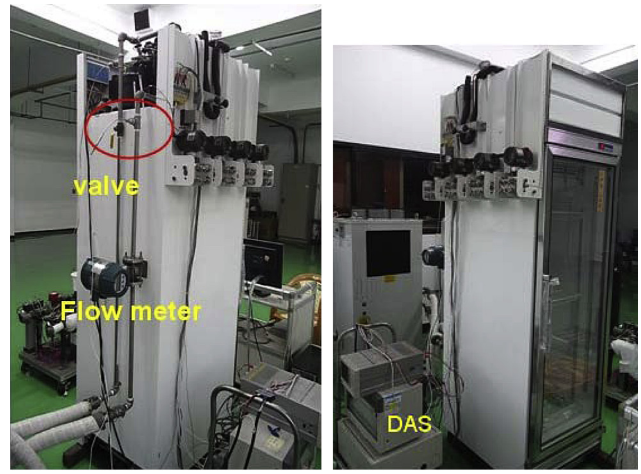

(a) Exterior (back view) . (b) Exterior (front view).

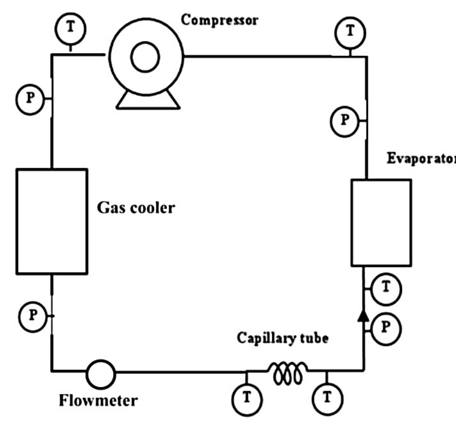

(c) Schematic of the system and sensor locations.

Fig. 4 – Schematics of the experimental CO_2 refrigerated cabinet and its components and measurements: (a) exterior (back view) (b) exterior (front view) (c) Schematic of the system and sensor locations. (a) COP_h. (b) Heating capacity.

Table 2a – Specifications of the gas cooler used for experimental testing.

Description	
Type of Heat exchanger	Tube-in-tube
Inner tube	CO_2
Outer tube	Water
ID of inner tube (mm)	12
OD of inner tube (mm)	18
ID of outer tube (mm)	27
Tube length (m)	2.58
Tube material	Copper
Solder	AISI 316

Table 2b – Specifications of the fin-and-tube heat exchanger used for experimental testing.

Description	
Heat exchanger type	Fin-and-tube heat exchanger
Transverse tube spacing (mm)	25.4
Longitudinal tube spacing (mm)	22
Outside tube diameter (mm)	9.52
Inside tube diameter (mm)	8.2
Tube material, tube arrangement	Cu, staggered
Fin spacing (mm)	4
Fin thickness (mm)	0.15
Number of tube rows	5
Number of tubes per row	4
Tube length (mm)	420

the gas cooler and evaporator with resolution up to 0.1 kPa. The inlet and outlet of the gas cooler and evaporator are measured by RTDs (Pt100Ω) having a calibrated accuracy of 0.1 °C. Some details of the geometric configurations of the gas cooler and the evaporator are shown in Table 2a and 2b. To verify the validity of the proposed simulation model of the transcritical CO_2 cycle, simulation results are then compared with those measured results from the experiment. The simulation results are obtained based on the same conditions of the experimental conditions which are listed in Table 3. The compressor speed is equal to the rated value with the system COP_h being defined as follows:

$$COP_h = \frac{Q_h}{W} \tag{42}$$

where W is the power consumption of the compressor, and Q_h is the heating capacity of the gas cooler. Fig. 5 shows the comparison of the predicted COP_h and the heating capacity against the measurements. As seen in Fig. 5, the predicted results are in favorable agreements with the experimental results. The maximum difference between the predicted and measured COP_h is 5.6% with a mean average difference of 2.2%. The results suggest the applicability of the proposed model. Hence, further detailed parametric calculations are made to explore the system response of the CO_2 transcritical cycle. The standard condition used for calculations is shown in Table 4a and the detailed geometrical configurations of the major components used for simulations are tabulated in Table 4b.

Table 3 – Test inlet conditions at the gas cooler and evaporator of the experimental run.

Variant	T_{db} (°C)	T_{wb} (°C)	$T_{w,i}$ (°C)	V_{fr} (m s^{-1})	$\dot{m}_w$ (kg s^{-1})
Run1	19.5	16.2	18.6	1.12	0.11
Run2	19.5	15.9	22.4	1.12	0.12
Run3	19.4	16.4	14.6	1.12	0.14
Run4	19	15.8	25.4	1.12	0.12
Run5	20.3	15.5	18.1	1.12	0.12
Run6	18.9	16.0	20.7	1.12	0.13
Run7	19.4	16.3	26.2	1.12	0.12
Run8	18.8	15.3	24.3	1.12	0.12
Run9	18.7	16.2	14.9	1.12	0.11
Run10	19.4	15.5	11.4	1.12	0.11
Run11	18.5	16.2	30.5	1.12	0.12
Run12	18.5	16.1	28.3	1.12	0.11

4. Results and discussion

The effect of the dry bulb temperature on the system performance is shown in Fig. 6. The corresponding mass flowrate of

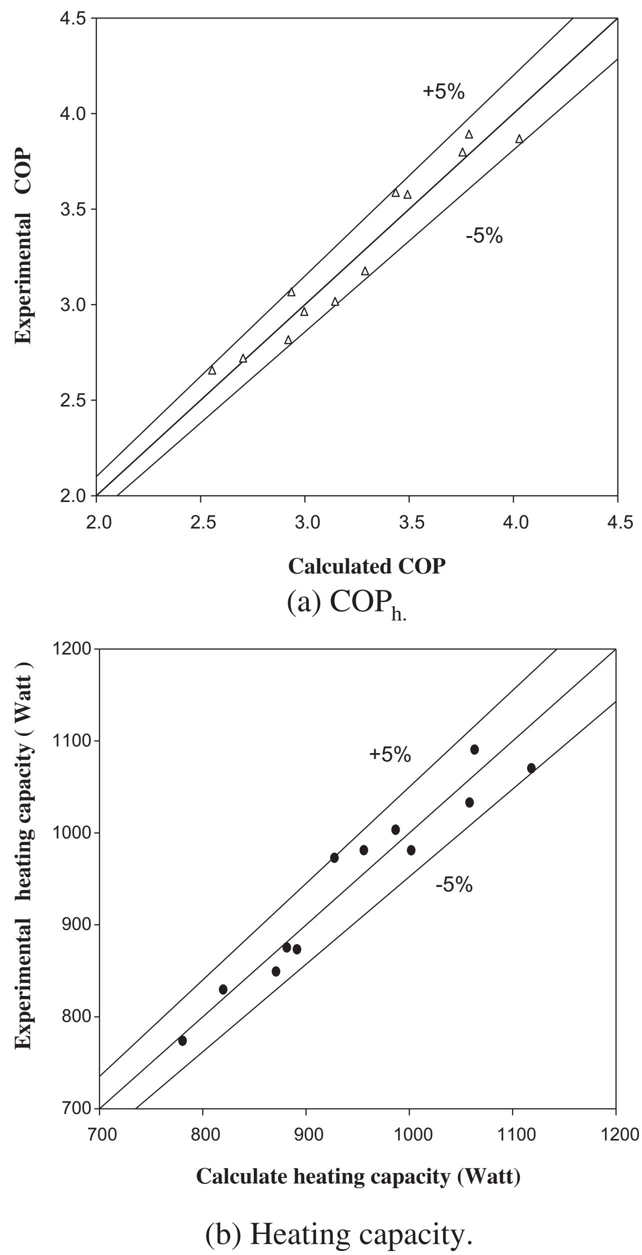

Fig. 5 – Comparison between the experimental measurements and simulations: (a) COP_h; (b) Heating capacity. (a) Variation of CO_2 mass flowrate. (b) Variation of system COP_h. (c) Variation of suction and discharge pressure. (d) Variation of heating capacity and power consumption.

Table 4a – Standard simulation conditions.

Water	Flow rate	kg s^{-1}	0.11–0.14
	Inlet temperature	°C	10–30
Air	Frontal velocity	m s^{-1}	1.12
	Inlet dry bulb temperature	°C	18–20
	Inlet wet bulb temperature	°C	15–17
Capillary tube	Length	m	5.0
Compressor	Diameter	mm	0.95
	Speed	rpm	3500
	Capacity	cc	1.5

the CO_2, the COP_h, the suction pressure, the discharge pressure, the heating capacity of the gas cooler, the cooling capacity of the evaporator, and the power consumption vs. inlet dry bulb temperature at the evaporator is shown in the figure. The results show that the system COP_h increases with the rise of the dry bulb temperature and the heating/cooling capacity of the gas cooler/evaporator also rise with the dry bulb temperature. However, the power consumption remains nearly the same. Moreover, the mass flowrate of the CO_2 and the pressure at the inlet and outlet of compressor tend to increase. The appreciable rise of mass flowrate of the CO_2 is the main reason of increasing heating capacity and the $COP_{h.}$ On the other hand, with a rise of the dry bulb temperature, it appears that the evaporation temperature is also increased, thereby leading to a rise of COP_h and the heating/cooling capacity. This is analogous to the conventional refrigerant system. Similar influence caused by raising the inlet frontal velocity is also seen in the figure. Despite the system performance is appreciably improved by raising the dry bulb temperature, the synchronous rise of the discharge pressure eventually place a upper limit on the dry bulb temperature due to the concerns of the mechanical failure. The effect of the relative humidity on the system performance subject to the inlet dry bulb temperature of 20 °C and 30 °C are shown in Fig. 7. The influence of the relative humidity is very similar to that of the dry bulb temperature. This is because the corresponding latent load rises when the relative humidity is increased, thereby leading to an appreciable rise of the evaporator temperature. Accordingly the increase of the relative humidity results in a higher discharge pressure and the system COP_h. However, it should be mentioned that the corresponding increase of the discharge pressure, suction pressure, and mass flowrate is less pronounced as compared to that of the dry bulb temperature. This is somehow expected for a fixed dry bulb temperature places an upper limit of the suction temperature.

Table 4b – Geometrical configurations of the major components for simulation.

Water	Mass flow rate	kg s^{-1}	0.08–0.20
	Inlet temperature	°C	5–30
Air	Flow rate	ms^{-1}	1.12
	Inlet temperature (dry bulb)	°C	15–30
	Inlet temperature (wet bulb)	°C	10–25
Capillary tube	Length	m	2.0
Compressor	Diameter	mm	1.8
	Rotary speed	rpm	3500
	Capacity	cc	14
Gas cooler	Inner tube ID	mm	12
	Inner tube OD	mm	18
	Outer tube ID	mm	27
Evaporator	Length	m	6.5
	Height	mm	677
	Width	mm	189.6
	Tube diameter	mm	7.35
	Transverse tube spacing	mm	25.4
	Longitudinal tube spacing	mm	19.05
	Fin spacing	mm	1.6
	Fin thickness	mm	0.115
	Number of tube row		2
	Number of tubes per row		7

Fig. 8 shows the effect of the inlet water temperature into the gas cooler on the system performance. The general system response subject to the inlet water temperature in the gas cooler is analogous to those of the dry bulb temperature. However, it appears that both of the system COP_h and the heating capacity are decreased with the rise of the inlet water temperature. The results are in line with the conventional refrigeration system that increasing the condensing temperature will result in a decrease of the system COP_h. Notice that raising the dry bulb temperature also leads to a rise of the discharge pressure at the gas cooler but it reveals a steady increase of the system COP_h. The main reason for the decreasing COP_h with respect to the effect of the inlet water temperature is associated with the difference in CO_2 refrigerant mass flowrate as shown in Fig. 8. When compared to the influence of the dry bulb temperature, it is found that the mass flowrate can be increased as much as 35% when the dry bulb temperature is increased from 15 to 30 °C. However, the rise of the mass flowrate is less than 8% when raising the water inlet temperature from 5 to 30 °C. The gigantic difference gives rise to a decrease of the heating capacity and the system COP_h. The other reason for decreasing COP_h is attributed to the dramatic change of thermophysical properties around the pseudocritical temperature. The decreasing trends subject to the inlet water temperature are in line with some existing experimental measurements, e.g. Stene (2005) and Goodman et al. (2011). Stene (2005) showed that the system COP_h is almost linearly decreased against the rise of the water coolant temperature, ranging from 12% to 25% when the inlet water temperature is raised from 5 to 30 °C. Analogous results were also reported by Goodman et al. (2011) who showed that the relative decline of the system COP_h, is about 30–40% when the inlet water temperature is raised from 5 to 35 °C. In Fig. 8, one can also see that the relative decline of the system COP_h for $\dot{m}_w = 0.2$ kg s^{-1} is more pronounced than that of $\dot{m}_w = 0.08$ kg s^{-1} despite $\dot{m}_w = 0.2$ kg^{-1} gives a higher heating capacity. This is attributed to a much better heat transfer performance of $\dot{m}_w = 0.2$ kg s^{-1} in the gas cooler that leads to a much lower pressure.

Fig. 9 shows the effect of the compressor speed on the mass flowrate of the CO_2, the system COP, the discharge pressure, the suction pressure, the heat transfer capacity of the gas cooler and the evaporator, and the power consumption. The results show that the system COP_h remarkably decreases with the compressor speed despite appreciable increases of the mass flowrate and the heating capacity are encountered. The

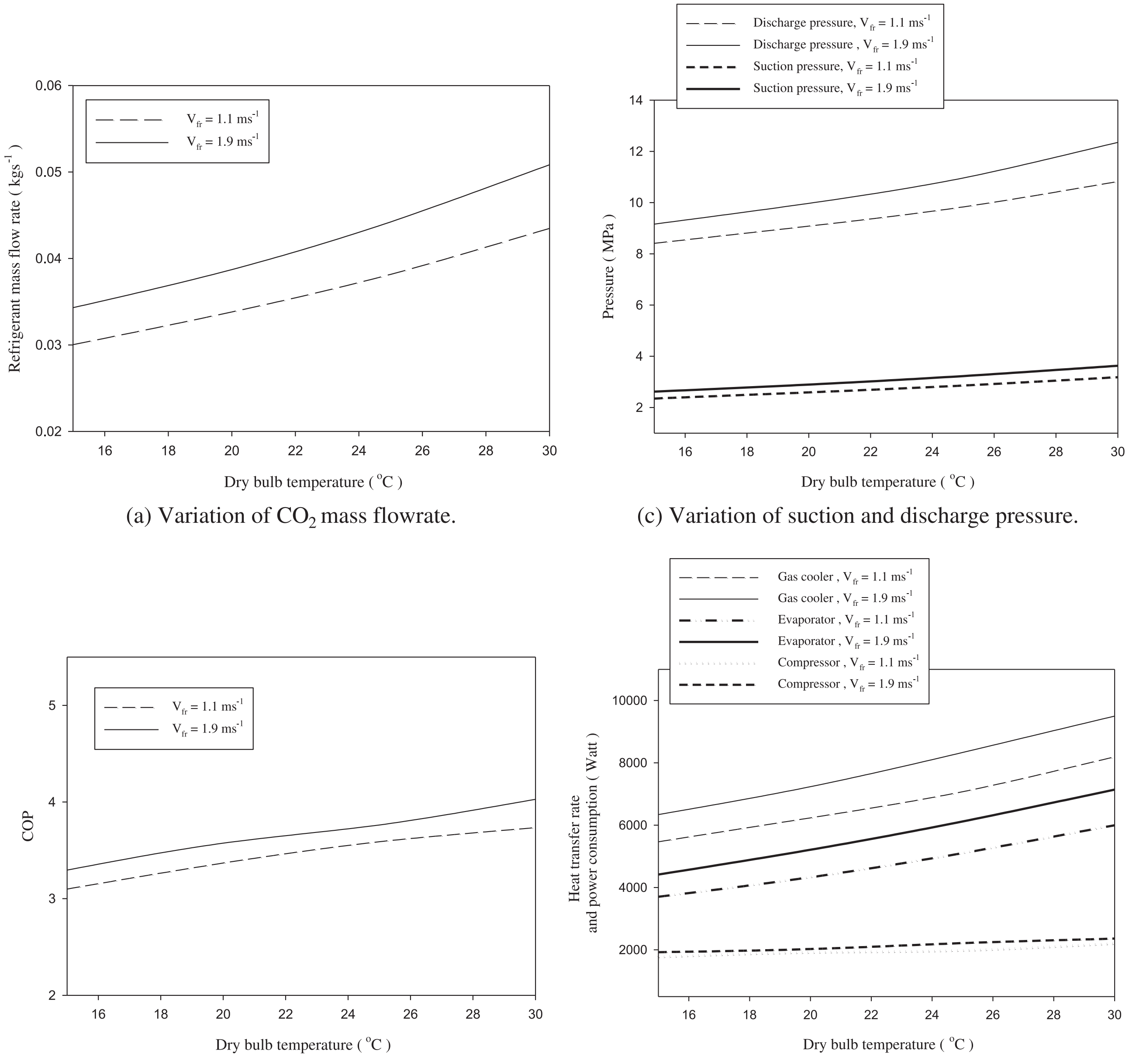

(a) Variation of CO_2 mass flowrate.

(c) Variation of suction and discharge pressure.

(b) Variation of system COP_h.

(d) Variation of heating capacity and power consumption.

Fig. 6 – Effect of the dry bulb temperature on (a) CO_2 mass flow rate; (b) COP_h; (c) discharge and suction pressure; (d) Heating capacity and power consumption. Simulation is performed with RH = 50%, $T_{w,i}$ = 10 °C, $\dot{m}_w$ = 0.08 kg s^{-1}, L_{cap} = 2.0 m, d_{cap} = 1.2 mm, N_{com} = 3500 rpm. (a) Variation of CO_2 mass flowrate. (b) Variation of system COP_h. (c) Variation of suction and discharge pressure. (d) Variation of heating capacity and power consumption.

sharp decline in COP_h is attributed to two major reasons. Firstly, a higher compressor speed leads to a larger compression ratio. In this case, the compression ratio varies from 1.8 to 3.2 as the compressor speed is increased from 1500 to 5000 rpm which suggests an approximately 15% decline of volumetric efficiency based on the evaluation from Eq. (40). On the other hand, the simultaneous increase of the discharge pressure and the decline of the suction pressure results in a considerable rise of the required compressor power. Consequently, a detectable deterioration of the COP_h emerges. Basically, the results are analogous to the conventional refrigeration system.

Fig. 10 shows the effect of the length of capillary tube on the system performance. As shown in the figure, it appears that the system COP_h shows a very slightly increases vs. the capillary tube length. Notice that the variation of the discharge and suction pressure is similar to that of increasing compressor speed. However, the rise of the discharge pressure and the decline of suction pressure are much smaller than that in increasing the compressor speed. The variations of the

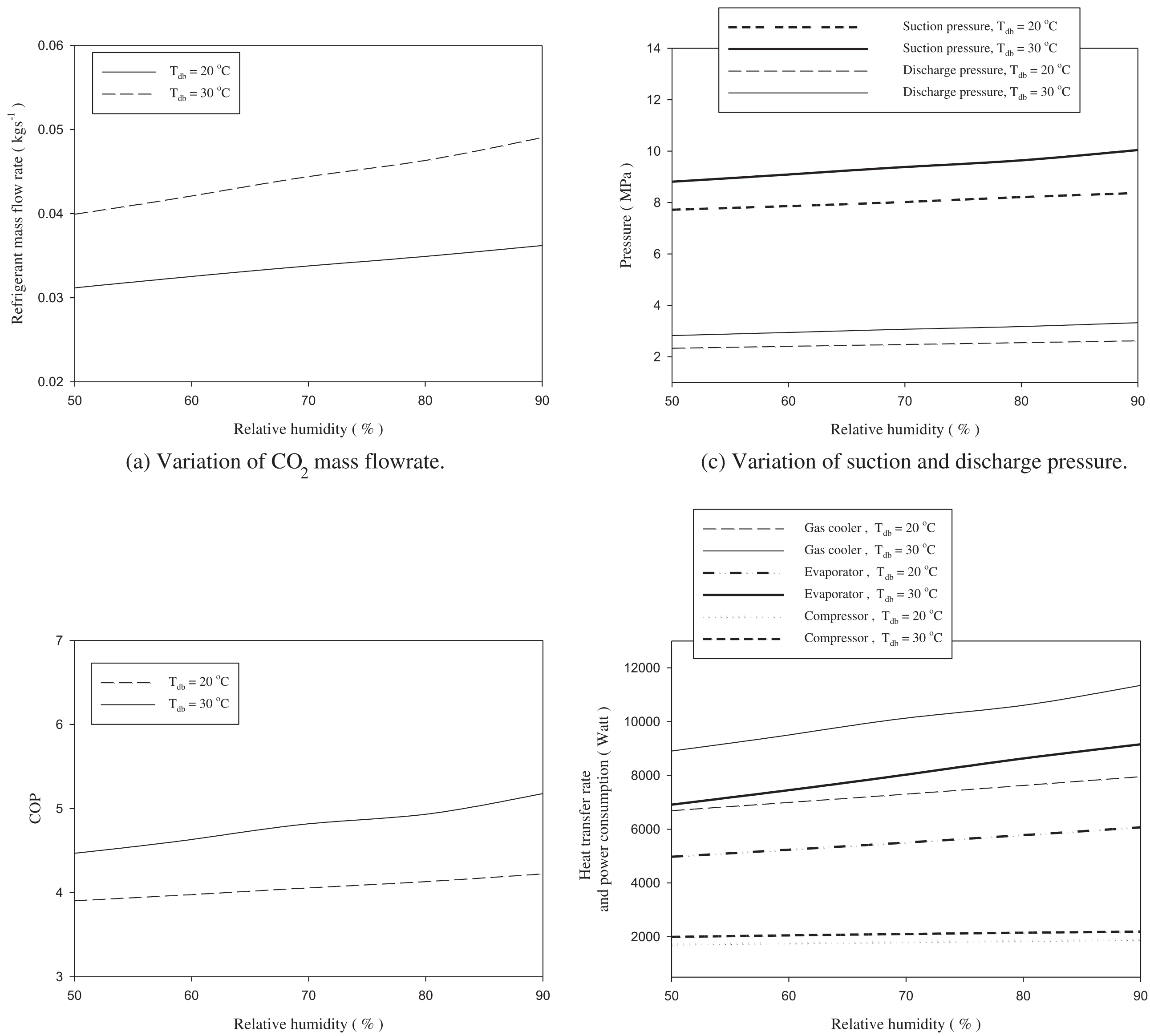

(a) Variation of CO_2 mass flowrate.

(c) Variation of suction and discharge pressure.

(b) Variation of system COP_h.

(d) Variation of heating capacity and power consumption.

Fig. 7 – Effect of the relative humidity on (a) CO_2 mass flow rate; (b) COP_h; (c) discharge and suction pressure; (d) Heating capacity and power consumption. Simulations are performed at $V_{fr} = 1.1$ m s^{-1}, $T_{wi} = 10$ °C, $\dot{m}_w = 0.2$ kg s^{-1}, $L_{cap} = 2.0$ m, $d_{cap} = 1.2$ mm, $N_{com} = 3500$ rpm. (a) Variation of CO_2 mass flowrate. (b) Variation of system COP_h. (c) Variation of suction and discharge pressure. (d) Variation of heating capacity and power consumption.

COP_h with the capillary tube length differ from those commonly observed in the conventional refrigeration system (e.g. Reddy et al., 2012). For a conventional refrigerant operated in the sub-critical region with a given capillary tube diameter, normally a maximum COP is attainable for a specific capillary tube length. Yet a detectable decrease of the COP is encountered if the capillary tube length is increased further. However, it is found that in the present transcritical operation where the COP_h reveals a continuous increase with respect to the capillary tube length. Even though the amount of increase is relatively small, but it shows no sign of achieving a maximum COP_h when the capillary tube length is increased from 0.5 to 3.5 m. To explain this unusual characteristic, one must resort to the difference of the variation of the enthalpy subject to the vapor pressure between the present CO_2 and the conventional refrigerant such as R-134a as shown in Fig. 11. For a conventional refrigerant like R-134a, the pressure rise results in a smaller enthalpy change since the major heat transfer mechanism in the condenser is latent heat as shown in Fig. 11(b). For instance, a 28% decrease in latent heat is observed for R-134a when the pressure is increased from 3 to 3.5 MPa. On the other hand, the enthalpy decline from 8 MPa to 10 MPa for the CO_2 in transcritical operation in the temperature span of 300–360 K is less than 4% as shown in

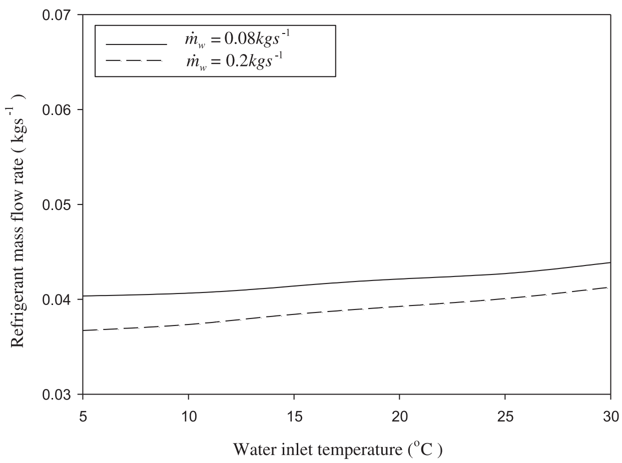

(a) Variation of CO_2 mass flowrate.

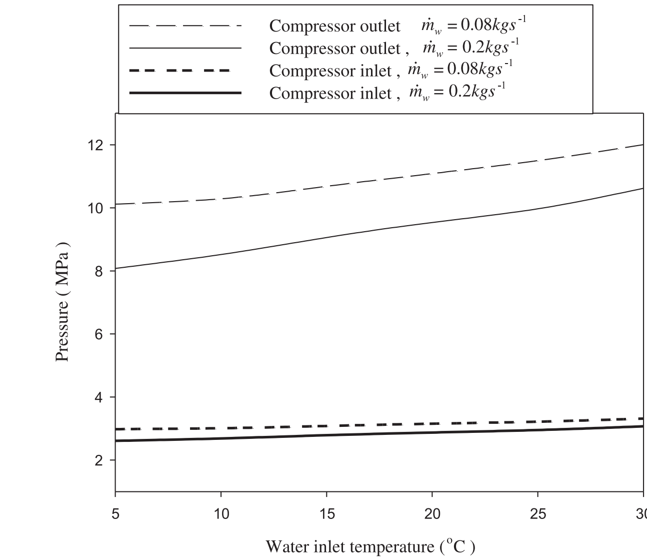

(c) Variation of suction and discharge pressure.

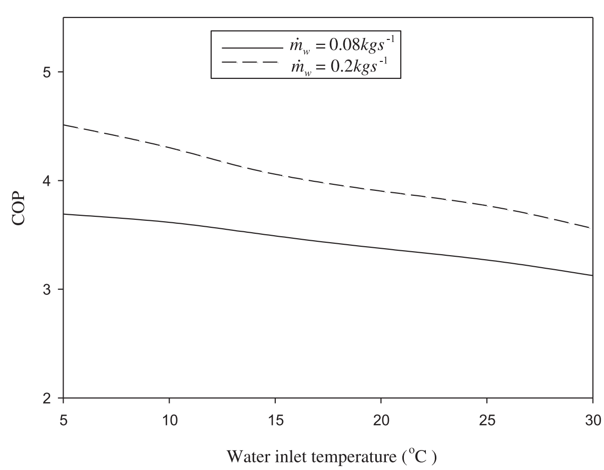

(b) Variation of system COP_h.

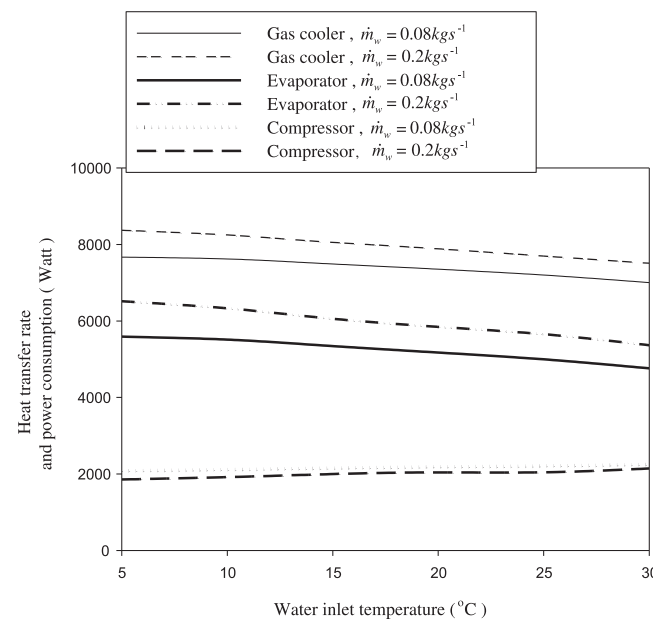

(d) Variation of heating capacity and power consumption.

Fig. 8 – Effect of the water inlet temperature at the gas cooler on (a) CO_2 mass flow rate; (b) COP_h; (c) discharge and suction pressure; (d) Heating capacity and power consumption. Simulations are performed at $T_{db} = 27\ ^\circ C$, $T_{wb} = 20\ ^\circ C$, $V_{fr} = 1.1\ m\ s^{-1}$, $L_{cap} = 2.0$ m, $d_{cap} = 1.2$ mm, $N_{com} = 3500$ rpm. (a) Variation of CO_2 mass flowrate. (b) Variation of system COP_h. (c) Variation of suction and discharge pressure. (d) Variation of heating capacity and power consumption.

Fig. 11(a). In addition, raising the discharge pressure of the CO_2 also accompanies with a significant increase of the CO_2 temperature, thereby the considerable rise of the temperature difference between the CO_2 and the water offsets the opposite influences of moderate decrease of the mass flowrate of CO_2. In summary of these two effects (higher temperature difference and a rather slight decrease in the enthalpy variation), the CO_2 system shows a slight increase of the heating capacity. Moreover, a moderate decrease in the mass flowate for a longer capillary tube length and a minor increase in the enthalpy change across the compressor bring about a nearly unchanged compressor power. In summary of the foregoing effects, the COP_h shows a very slight increase against the length of the capillary tube. Note that increasing the capillary tube length results in a higher discharge pressure and a lower suction pressure which is similar to that of increasing compressor speed. However, the mass flowrate in the former is decreasing while the latter is increasing. Yet the required

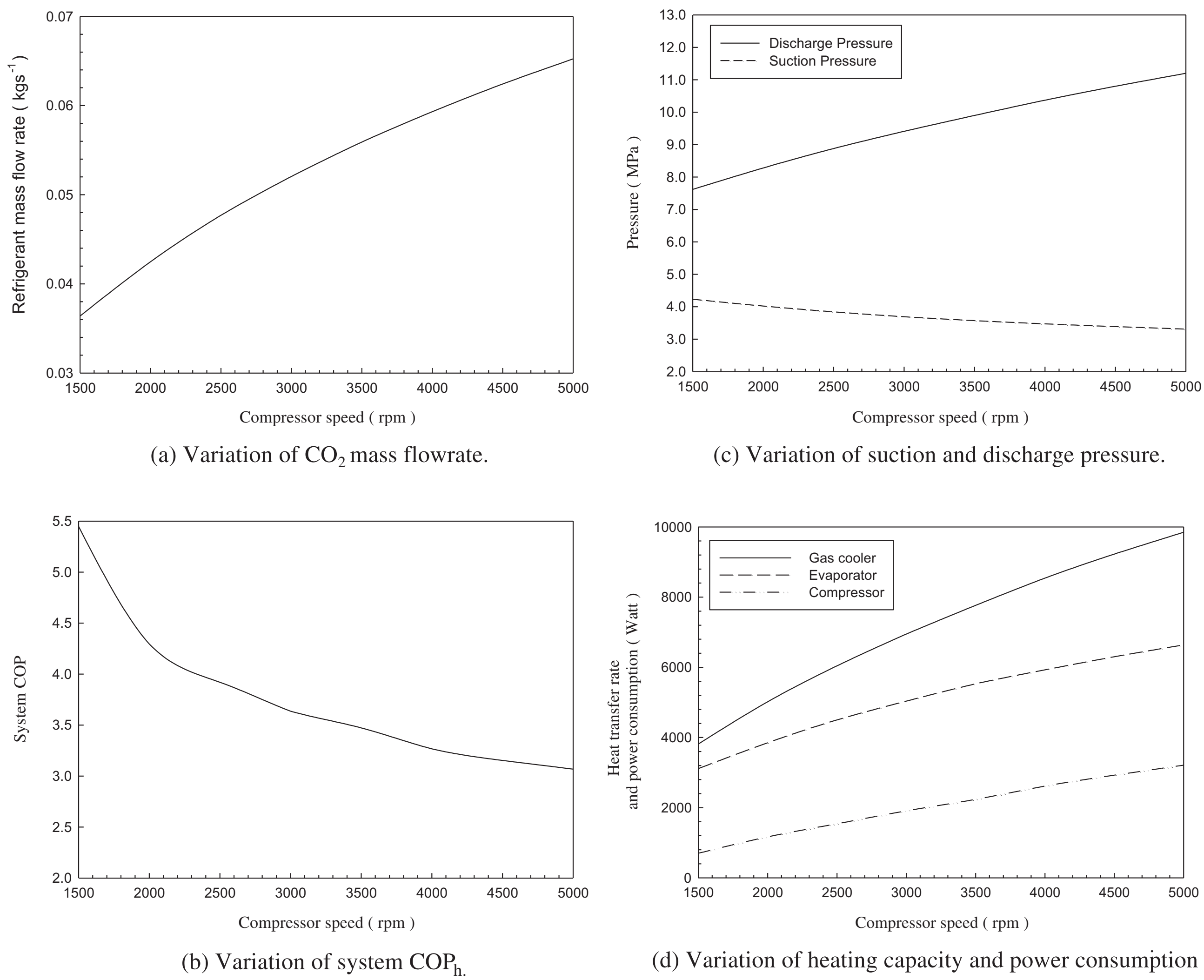

Fig. 9 – Effect of the compressor speed on (a) CO_2 mass flow rate; (b) COP_h; (c) discharge and suction pressure; (d) Heating capacity and power consumption. Simulation is performed with $T_{db} = 27\ ^\circ C$, $T_{wb} = 20\ ^\circ C$, $T_{w,i} = 10\ ^\circ C$, $\dot{m}_w = 0.2\ kg\ s^{-1}$, $L_{cap} = 2.0\ m$, $d_{cap} = 1.4\ mm$. (a) Variation of CO_2 mass flowrate. (b) Variation of system COP_h. (a) Variation of suction and discharge pressure. (d) Variation of heating capacity and power consumption.

compressor work in the former remains unchanged while it is appreciably increased in the latter. As a consequence, one can see a dramatic difference in COP_h between these two cases.

5. Concluding remarks

In this study a system model capable of handling the system response of a CO_2 transcritical cycle is proposed. Unlike some existing system models applicable for the CO_2, the present model does not impose any excessive constraints such as fixed discharge pressure, suction pressure, and so on during the modeling. In addition, the complex configurations of the heat exchangers, including detailed geometrical variation of the gas cooler and fin-and-tube evaporator have been taken into account to make the simulation quite realistic. The system simulation is first compared with the experimental measurements and good agreements between the simulation and the measurements are reported. For further examinations the system response of the CO_2 transcritical cycle, parametric studies on the system performance with regard to the effect of dry bulb temperature, relative humidity in the evaporator, inlet water temperature at the gas cooler, compressor speed, and the capillary tube length are reported. The associated parametric influences on the CO_2 transcritical system are summarized in the following:

(1) The system COP_h, and the heating capacity increases with the rise of the inlet dry bulb temperature in the evaporator. However, the discharge pressure also rises considerably against the dry bulb temperature.
(2) The effect of the relative humidity in the evaporator on the system performance is similar to that of the dry bulb temperature. The system COP_h, the heating capacity, and

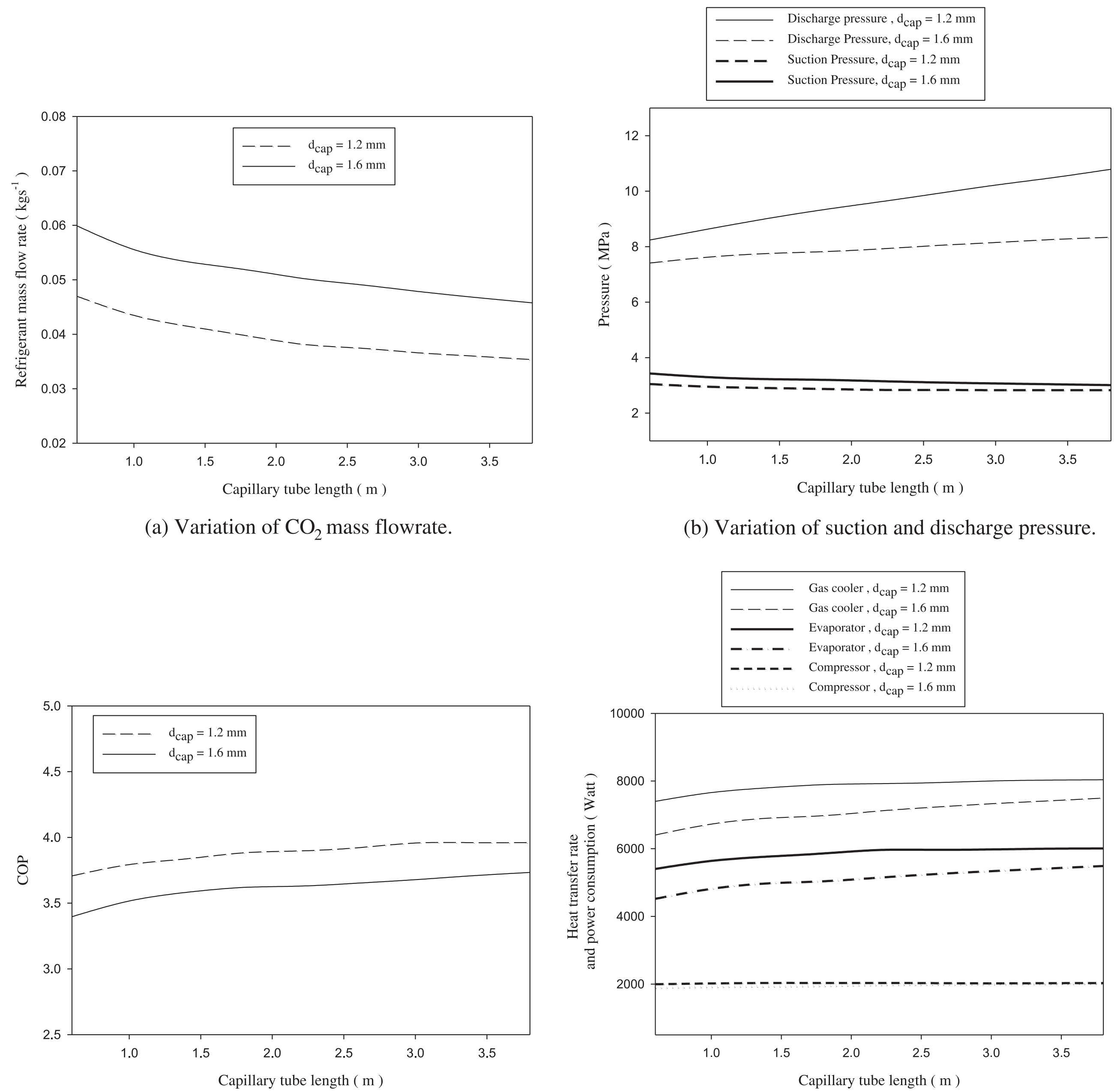

(a) Variation of CO_2 mass flowrate.

(b) Variation of suction and discharge pressure.

(b) Variation of system COP_h.

(d) Variation of heating capacity and power consumption

Fig. 10 – Effect of the capillary tube length on (a) CO_2 mass flow rate; (b) COP_h; (c) discharge and suction pressure; (d) Heating capacity and power consumption. Simulation is performed with $T_{db} = 27\ ^\circ C$, $T_{wb} = 20\ ^\circ C$, $T_{w,i} = 20\ ^\circ C$, $V_{fr} = 1.1\ m\ s^{-1}$, $\dot{m}_w = 0.2\ kg\ s^{-1}$, $N_{com} = 3500$ rpm.

the discharge pressure also increase with the rise of the relative humidity due to increase of latent loading but the increase is less pronounced as compared to that of the dry bulb temperature.

(3) It is found that the inlet water temperature at the gas cooler casts significant impact on this system performance. Despite the CO_2 mass flowrate may be increased with the inlet water temperature, the system COP_h declines considerably with the inlet water temperature.

(4) The rise of the compressor speed will give rise to a higher heating capacity but it also leads to a much lower COP_h due to a substantial increase of the compressor work.

(5) Unlike those of the conventional sub-critical refrigerant, the system COP_h does not reveal a maximum value against the capillary tube length. This is mainly due to a much smaller enthalpy change for the CO_2 transcritical operation.

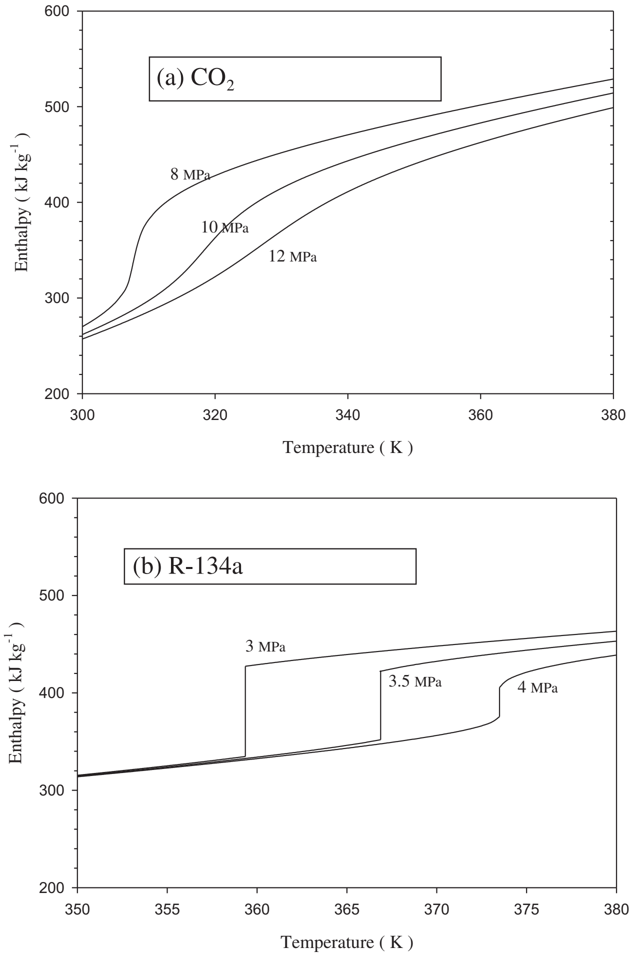

Fig. 11 – Schematic of the enthalpy change vs. temperature at various system pressures for (a) CO_2; and (b) R-134a.

Acknowledgments

This work is supported by the National Science Council of Taiwan under contract of 102-ET-E-009-006-ET. The financial support from the Bureau of Energy from the Ministry of Economic Affairs, Taiwan is also highly appreciated.

REFERENCES

Agrawal, N., Bhattacharyya, S., Nanda, P., 2011. Flow characteristics of capillary tube with CO_2 transcritical refrigerant using new viscosity models for homogeneous two-phase flow. Int. J. Low-Carbon Tech. 6, 243–248.

Aprea, C., Maiorino, A., 2009. Heat rejection pressure optimization for a carbon dioxide split system: an experimental study. Appl. Energy 86, 2373–2380.

Bump, T.R., 1963. Average temperatures in simple heat exchanger. ASME J. Heat Transfer 85, 182–183.

Cabello, R., Sánchez, D., Llopis, R., Torrell, E., 2008. Experimental evaluation of the energy efficiency of a CO_2 refrigerating plant working in transcritical conditions. Appl. Therm. Eng. 28, 1596–1604.

Dang, C., Hihara, E., 2004. In-tube cooling heat transfer of supercritical carbon dioxide part 1: experimental measurement. Int. J. Refrigeration 24, 736–747.

Gnielinsk, V., 1976. New equation for heat and mass transfer in turbulent pipe and channel flow. Int. Chem. Eng. 16, 359–368.

Goodman, C., Fronk, B.M., Garimella, S., 2011. Transcritical carbon dioxide microchannel heat pump water heaters: Part II - system simulation and optimization. Int. J. Refrigeration 34, 870–880.

Hihara, E., Tanaka, S., 2000. Boiling heat transfer of carbon dioxide in horizontal tubes. In: Proceedings of the 4th IIR Gustav Lorentzen Conference on Natural Working Fluids, pp. 279–284.

Kim, S.G., Kim, Y.J., Lee, G., Kim, M.S., 2005. The performance of a transcritical CO_2 cycle with an internal heat exchanger for hot water heating. Int. J. Refrigeration 28, 1064–1072.

Lin, S., Kwok, C.C.K., Li, R.Y., 1991. Local friction pressure drop during vaporization of R-12 through capillary tubes. Int. J. Multiphase Flow 17, 95–102.

Lin, Y.T., Hsu, K.C., Chang, Y.J., Wang, C.C., 2001. Performance of rectangular fin in wet conditions: visualization and wet fin efficiency. ASME J. Heat Transfer 123, 827–836.

Lockhart, R.W., Martinelli, R.C., 1949. Proposed correlation of data for isothermal twophase, two-component flow in pipes. Chem. Eng. Prog. 45, 39–48.

Lorentzen, G., 1994. Revival of carbon dioxide as a refrigerant. Int. J. Refrigeration 17, 292–300.

Lorentzen, G., 1995. The use of natural refrigerants: a complete solution to the CFC/HCFC predicament. Int. J. Refrigeration 18, 190–197.

Lorentzen, G., Pettersen, J., 1993. A new, efficient and environmentally benign system for car air conditioning. Int. J. Refrigeration 16, 4–12.

McAdams, W.H., Woods, W.K., Bryan, R.L., 1942. Vaporization inside horizontal tubes-II-Benzene-oil mixtures. Trans. ASME 64, 93–200.

Myers, R.J., 1967. The Effect of Dehumidification on the Air-side Heat Transfer Coefficient for a Finned-tube Coil. M. S. thesis. University of Minnesota Minneapolis.

Reddy, D.V.R., Bhramara, P., Govindarajulu, K., 2012. Performance and optimization of capillary tube length in a split type air conditioning system. Int. J. Eng. Res. Tech. 1 (7), 1–11.

REFPROP, 2007. Thermodynamic Properties of Refrigerants and Refrigerant Mixtures, Version 8.0. National Institute of Standards and Technology, Gaithersburg, M.D.

Riffat, S.B., Alfonso, C.F., Oliveira, A.C., Reay, D.A., 1996. Natural refrigerants for refrigeration and air-conditioning systems. Appl. Therm. Eng. 17, 33–41.

Sarkar, J., Bhattacharyya, S., Ramgopal, M., 2004. Optimization of a transcritical CO_2 heat pump cycle for simultaneous cooling and heating applications. Int. J. Refrigeration 27, 830–838.

Sarkar, J., Bhattacharyya, S., Ramgopal, M., 2006. Simulation of a transcritical CO_2 heat pump cycle for simultaneous cooling and heating applications. Int. J. Refrigeration 29, 735–743.

Sarkar, J., Bhattacharyya, S., Ramgopal, M., 2009. A transcritical CO_2 heat pump for simultaneous water cooling and heating: test results and model validation. Int. J. Energy Res. 33, 100–109.

Sarkar, J., Bhattacharyya, S., Ramgopal, M., 2010. Performance of a transcritical CO_2 heat pump for simultaneous water cooling and heating. Int. J. Appl. Sci. 6, 57–63.

Stene, J., 2005. Residential CO_2 heat pump system for combined space heating and hot water heating. Int. J. Refrigeration 28, 1259–1265.

Threlkeld, J.L., 1970. Thermal Environmental Engineering. Prentice-Hall, Inc, New-York.

Wang, C.C., 2000. Recent progress on the air-side performance of fin-and-tube heat exchangers. Int. J. Heat Exchangers 1, 49–76.

Wang, C.C., Hsieh, Y.J., Lin, Y.T., 1997. Performance of plate finned tube heat exchangers under dehumidifying conditions. ASME J. Heat Transfer 119, 109–117.

Wang, C.C., Lee, W.S., Sheu, W.J., Liaw, J.S., 2001. Empirical airside correlations of fin-and-tube heat exchangers under dehumidifying conditions. Int. J. Heat Exchangers 2, 54–80.

Wang, F.K., Fan, X.W., Zhang, X.P., Lian, Z.W., 2009. Modeling and simulation of a transcritical R744 heat pump system. In: 4th IEEE Conference on Industrial Electronics and Applications, 25–27 May 2009. ICIEA 2009, pp. 3192–3196.

Yamaguchi, S., Kato, D., Saito, K., Kawai, S., 2011. Development and validation of static simulation model for CO_2 heat pump. Int. J. Heat Mass Transf. 54, 1896–1906.

Yang, J.L., Ma, Y.T., Li, M.X., Hua, J., 2010. Modeling and simulating the transcritical CO_2 heat pump system. Energy 35, 4812–4818.

Yokoyama, R., Shimizu, T., Ito, K., Takemura, K., 2007. Influence of ambient temperatures on performance of a CO_2 heat pump water heating system. Energy 32, 388–398.

Yu, P.Y., Lin, K.H., Lin, W.K., Wang, C.C., 2012. Performance of a tube-in-tube CO_2 gas cooler. Int. J. Refrigeration 35, 2033–2038.